ASCA OBSERVATIONS OF THE SAGITTARIUS B2 CLOUD: AN X-RAY REFLECTION NEBULA

HIROSHI MURAKAMI,[1] KATSUJI KOYAMA,[2] MASAAKI SAKANO,[1] AND MASAHIRO TSUJIMOTO

Department of Physics, Faculty of Science, Kyoto University, Sakyo-ku, Kyoto 606-8502, Japan; hiro@cr.scphys.kyoto-u.ac.jp,
koyama@cr.scphys.kyoto-u.ac.jp, sakano@cr.scphys.kyoto-u.ac.jp, tsujimot@cr.scphys.kyoto-u.ac.jp

AND

YOSHITOMO MAEDA[1]

Department of Astronomy and Astrophysics, Pennsylvania State University, University Park, PA 16802-6305; maeda@astro.psu.edu

ABSTRACT

We present the ASCA results of imaging spectroscopy of the giant molecular cloud Sgr B2. The X-ray spectrum is found to be very peculiar; it exhibits a strong emission line at 6.4 keV, a low-energy cutoff below about 4 keV, and a pronounced edge structure at 7.1 keV. The X-ray image is extended, and its peak position is shifted from the core of the molecular cloud toward the Galactic center by about 1′–2′. The X-ray spectrum and the morphology are well reproduced by a scenario that X-rays from an external source located in the Galactic center direction are scattered by the molecular cloud Sgr B2 and come into our line of sight. Thus, Sgr B2 may be called an *X-ray reflection nebula*. Possible implications of the Galactic center activity related to this unique source are presented.

Subject headings: Galaxy: abundances — Galaxy: center — ISM: clouds —
ISM: individual (Sagittarius B2) — X-rays: ISM

1. INTRODUCTION

X-rays from the Galactic center (GC) region have been repeatedly observed with past X-ray instruments. One of the remarkable discoveries is a large-scale hot plasma of about 100 pc in diameter, which is associated with prominent Kα lines of He- or H-like irons (Koyama et al. 1989; Yamauchi et al. 1990). The total energy of the large-scale plasma is about 10^{54} ergs, with a dynamical age of $\sim 10^5$ yr. The ASCA satellite, with imaging capability in the wide energy band (0.5–10 keV) and reasonable energy resolution, has further found a high-temperature plasma inside the Sgr A shell (an oval region of $\sim 2' \times 3'$) with the total energy of 3×10^{50} ergs (Koyama et al. 1996). Using the size of ~ 4 pc and temperature of ~ 10 keV (Koyama et al. 1996), we estimate the dynamical age of the smaller plasma to be $\sim 10^3$ yr.

ASCA also found diffuse emission from the 6.4 keV neutral iron line; the brightest region is located over the giant molecular cloud Sgr B2, but its X-ray peak is shifted toward the GC from that of the molecular gas (Koyama et al. 1996). Koyama et al. (1996) speculated that the Galactic nucleus Sgr A* had been bright until some hundreds of years ago, the light-travel time between Sgr B2 and Sgr A*, but is currently dim. This putative activity in the past may also explain the oval-shape plasma surrounding Sgr A*, because the dynamical age of the plasma is about 10^3 yr.

The 6.4 keV line regions, together with the hot plasma surrounding Sgr A*, may thus provide a challenging scenario for the past activity of the GC. However, the previous report was based on limited data sets, hence their interpretations were rather preliminary and qualitative. We therefore have analyzed the X-ray spectrum and morphology of the Sgr B2 cloud in further detail, combining all the available data, and we try to give more quantitative results and implications.

With the combined analysis of the CO molecular lines and the far-infrared dust emissions, the mass of Sgr B2 is estimated to be $6 \times 10^6 \, M_\odot$ within a region of ~ 45 pc in diameter (Lis & Goldsmith 1989), hence it is one of the largest molecular clouds in the Galaxy.

We assume the distance to Sgr B2 is the same as that to the GC (Sgr A*), or 8.5 kpc, which is within an error of estimated distance of 7.1 ± 1.5 kpc (Reid et al. 1988). Then the distance between Sgr B2 and Sgr A* is about 100 pc.

2. OBSERVATIONS

Two observations of Sgr B2 were made with ASCA on 1993 October 1 and on 1994 September 22–24. In both observations, all four detectors, two solid-state imaging spectrometers (SIS0, SIS1), and two gas imaging spectrometers (GIS2, GIS3) were operated in parallel, hence four independent data sets were provided. Details of the instruments, the telescopes and the detectors, are found in Tanaka, Inoue, & Holt (1994), Serlemitsos et al. (1995), Burke et al. (1991), Ohashi et al. (1996), Makishima et al. (1996), and Gotthelf (1996). Each of the GIS was operated in PH mode with the standard bit assignment. The SIS data were obtained in 4-CCD bright mode. The data were postprocessed to correct for spatial-gain nonlinearity. Data taken at geomagnetic cutoff rigidities lower than 6 GeV c^{-1}, at elevation angles less than 10° for the GIS and 5° for the SIS from the Earth rim, or during the passage through the South Atlantic Anomaly were excluded. For the SIS, we also excluded the data taken at elevation angles from the bright Earth rim less than 25°. After these filters were applied, the net observing times were 95 ks for the GIS and 85 ks for the SIS.

3. RESULTS

Koyama et al. (1996) have already reported that the Sgr B2 cloud region is particularly bright in the 6.4 keV line. We

---

[1] Research Fellow of the Japan Society for the Promotion of Science (JSPS).
[2] CREST, Japan Science and Technology Corporation (JST), 4-1-8 Honmachi, Kawaguchi, Saitama 332-0012, Japan.

therefore made X-ray images in narrow energy bands with a central energy of 6.4 keV and width of twice the energy resolution (FWHM): 5.8–7.0 keV for the GIS and 6.2–6.6 keV for the SIS. Figure 1a shows the narrowband SIS image laid over the radio intensity contours of the CH_3CN line (Bally et al. 1988) and Figure 1b the GIS image. Since the SIS image is already found in Figure 3b in Koyama et al. (1996), we present the combined image of the two observations.

3.1. *Spectrum of Sgr B2*

For the X-ray spectrum we mainly used the GIS data, because in the high-energy band, including the iron K shell line, the GIS provides better statistics than the SIS. The GIS spectrum given in Figure 2 is obtained by summing the X-ray photons in 3′ radius circles around the X-ray peaks of the GIS images. For the background spectrum, we used an elliptical region with the major axis parallel to the Galactic plane, excluding the region of Sgr B2 (a 3′ radius circle) and the other X-ray bright spot (the other 3′ radius circle) at the west of Sgr B2. The source and the background regions are shown in Figure 1b with the filled circle and dotted ellipse, respectively.

In order to derive a quantitative feature of the Sgr B2 X-rays, we fitted the spectrum to two phenomenological models, a thermal bremsstrahlung and a power-law model, each with a Gaussian line. We used the Morrison & McCammon (1983) cross section for the absorption. Because of large absorption at low energy, the available data to be fitted are in the 4.0–10.0 keV band. However, the limited energy band and rather poor statistics do not allow us to constrain either model. Therefore, we assumed a power law of (fixed) photon index 2.0 (Koyama et al. 1996). The best-fit parameters are given in Table 1. As we expected, the 6.4 keV line is very strong with an equivalent width of 2.9 keV. The hydrogen column density is $N_H \sim 8 \times 10^{23}$ H cm^{-2}, and the luminosity is $\sim 10^{35}$ ergs s^{-1} (here and elsewhere all X-ray luminosities are corrected for absorption unless otherwise noted).

We also made an SIS spectrum and fitted it with the same model of the GIS. However, since the limited photon statistics prevented us from determining the absorption depth, we fixed the hydrogen column to the best-fit value for the GIS. The results given in Table 1. The SIS results were found to be consistent with the GIS. The narrow field of view of SIS severely constrains the selection of the back-
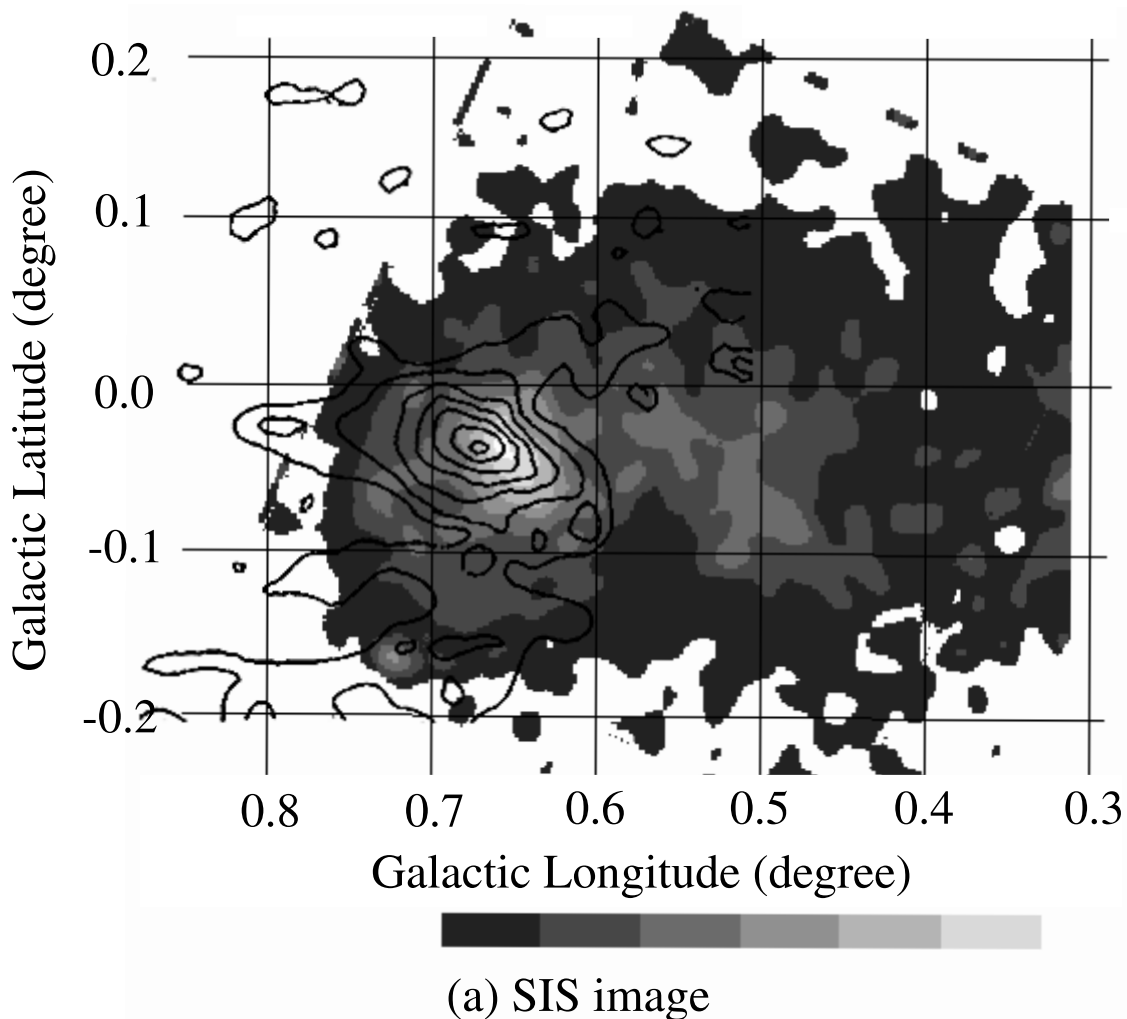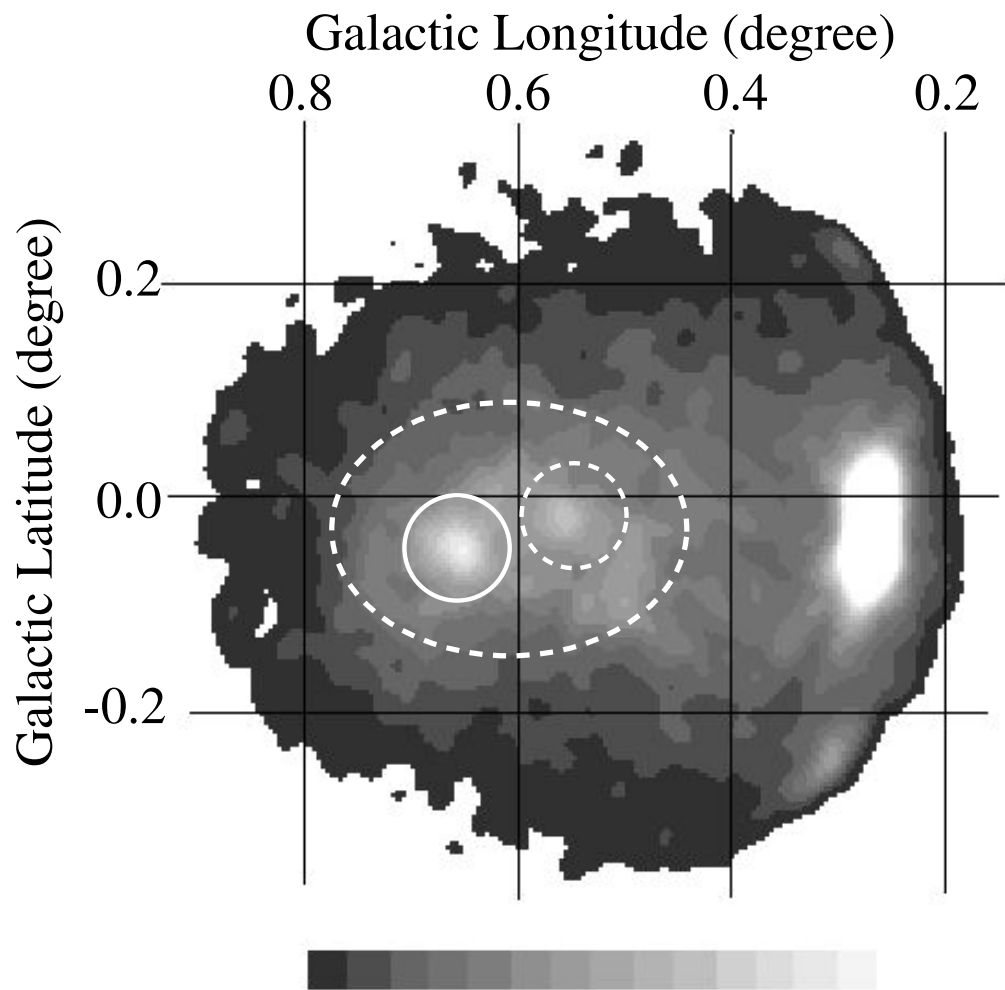

(a) SIS image

Fig. 1.—(a) The 6.4 keV line image around the Sgr B2 cloud obtained with the SIS, laid over the CH_3CN line contours (Bally et al. 1988). The 6.4 keV brightness distribution is shifted from the radio distribution by ∼1′.2 to the GC side (to the right in the figure). (b) The 6.4 keV line image with the GIS. The source and the background regions are shown by the filled circle and the dotted ellipse, respectively. The dotted circle encloses the other X-ray bright spot, which is excluded from the background region. The bright source at the boundary is a galactic binary X-ray source (1E 1743.1−2843).

Galactic Longitude (degree)

(b) GIS image

Fig. 1.—*Continued*

ground region for the SIS spectrum and increases background-subtraction uncertainties. Thus, here and after, we analyzed only the GIS spectrum for more detailed studies.

Koyama et al. (1996) reported that the most prominent iron K lines from the GC region are the 6.4 keV line from cold iron and the 6.7 keV line from He-like iron. Accordingly, we fitted the spectrum to the power law and two narrow Gaussian lines at 6.4 and 6.7 keV and found no significant line at 6.7 keV, with the flux less than 10% of the 6.4 keV line. Thus, the observed line profile is reproduced by the 6.4 keV line alone.

TABLE 1

FITTING RESULTS OF SGR B2 TO A PHENOMENOLOGICAL SPECTRAL MODEL

Model Components	GIS	SIS
Absorption (N_H[a]) (H cm^{-2})	$8.3^{+2.5}_{-2.0} \times 10^{23}$	8.3×10^{23} (fixed)
Continuum:		
Photon index	2.0 (fixed)	2.0 (fixed)
Flux[b] (4–10 keV) (photon s^{-1} cm^{-2})	$1.5^{+0.3}_{-0.2} \times 10^{-4}$	$1.8^{+0.6}_{-0.6} \times 10^{-4}$
Fe 6.4 keV line:		
Center energy (keV)	$6.38^{+0.03}_{-0.03}$	$6.43^{+0.02}_{-0.03}$
Flux[b] (photon s^{-1} cm^{-2})	$9.7^{+1.0}_{-1.0} \times 10^{-5}$	$9.7^{+1.7}_{-1.7} \times 10^{-5}$
Equivalent width (keV)	$2.9^{+0.3}_{-0.9}$	$2.1^{+2.1}_{-0.8}$
Total luminosity ($L_{4-10 \text{ keV}}$) (ergs s^{-1})	$1.1^{+0.7}_{-0.5} \times 10^{35}$	$1.4^{+0.7}_{-0.9} \times 10^{35}$
Reduced χ^2 (dof)	0.91 (34)	0.78 (45)

NOTE.—Errors are at 90% confidence level.
[a] Equivalent hydrogen column density for the solar abundances.
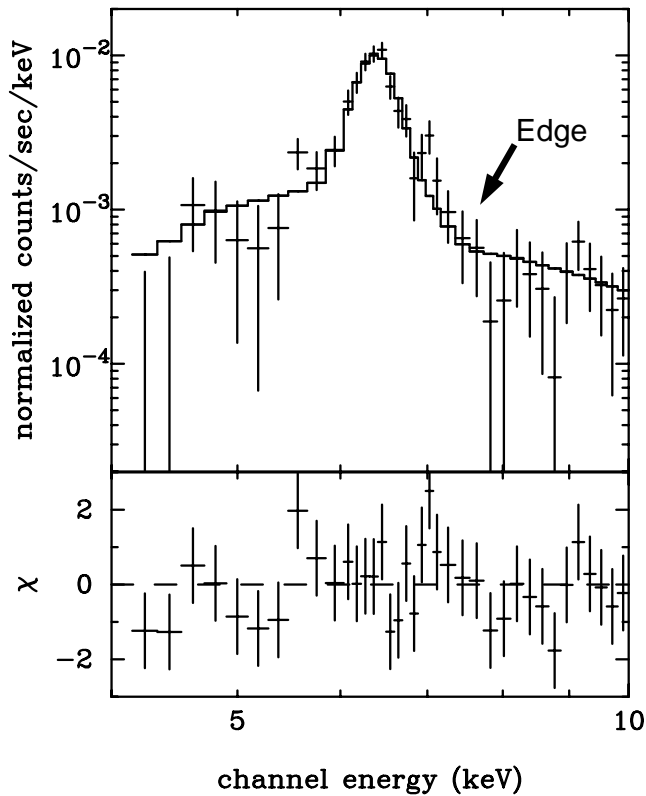[b] Fluxes are not corrected for absorption.

FIG. 2.—GIS (GIS2+GIS3) spectrum of Sgr B2. The solid line shows the simulated spectrum of an XRN (see § 4.2) after the convolution of the response function.

The observed hydrogen column of 8×10^{23} H cm^{-2} is at least 5 times larger than that of interstellar gas to the GC region (Sakano et al. 1997). This means that the large absorption column is due to local gas near or at the Sgr B2 cloud.

We found a deep iron edge in the spectrum. We fitted the spectrum allowing the iron column density to be free. Then the iron column density is estimated to be 4×10^{19} Fe cm^{-2}.

3.2. X-Ray Morphology

To determine accurate X-ray peak positions, we made projected X-ray intensity profiles (6.2–6.6 keV) on the right ascension (R.A.) and declination (decl.) axes and fitted to a phenomenological model function: Gaussian plus exponential tails for the two sides. Each of the best-fit positions of the X-ray peak, thus determined in the GIS and the SIS images, are R.A. (2000) = 17$^{\rm h}$47$^{\rm m}$20$^{\rm s}$5, decl. (2000) = $-28°24'20''$ and R.A. (2000) = 17$^{\rm h}$47$^{\rm m}$20$^{\rm s}$3, decl. (2000) = $-28°24'13''$, respectively, with statistical errors of 10$''$ for the GIS and 15$''$ for the SIS. Although the SIS has a better spatial resolution than the GIS, it shows a larger error, due mainly to the poor photon statistics compared with the GIS. An additional, but even larger, error is uncertainty in the *ASCA* attitude determination, which is less than 40$''$ (Gotthelf 1996).

The radio peak of Sgr B2 is R.A. (2000) = 17$^{\rm h}$47$^{\rm m}$20$^{\rm s}$1, decl. (2000) = $-28°23'6''$ in 4$''$5 × 3$''$7 beam size from the HC$_3$N observation by Lis et al. (1993). Thus the X-ray peak is shifted from the cloud core to the south by 1$'$2, which is significantly larger than the X-ray position errors.

Spatial extent of the 6.4 keV line and the continuum X-ray images are examined with the SIS data, because spatial resolution of the SIS is better than that of the GIS. We made radial profiles for the 6.2–6.6 keV and the 4.0–10.0 keV (excluding the 6.2–6.6 keV band) bands; the former band is dominated by the 6.4 keV line photons while the latter represents the continuum X-ray photons. For comparison we simulated the point-spread function (PSF) by the ray-tracing code (Kunieda et al. 1995). Then we fitted the PSF to the observed radial profiles with two free parameters of normalization and background level and found the
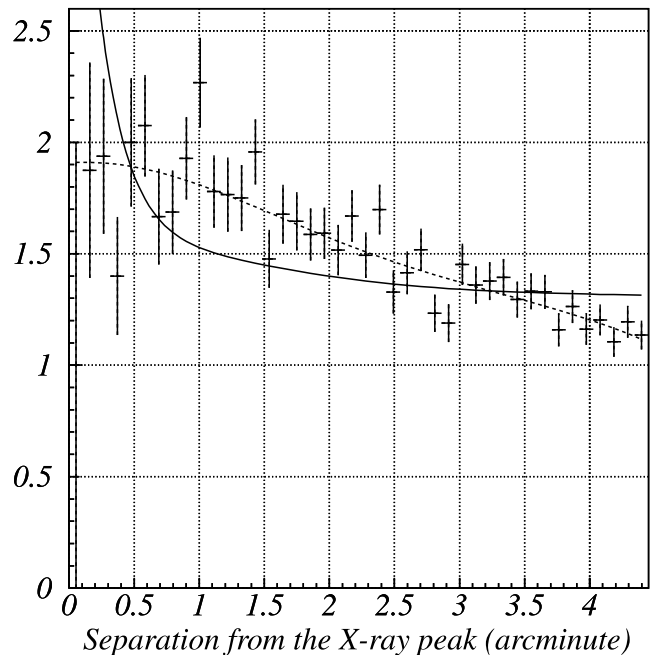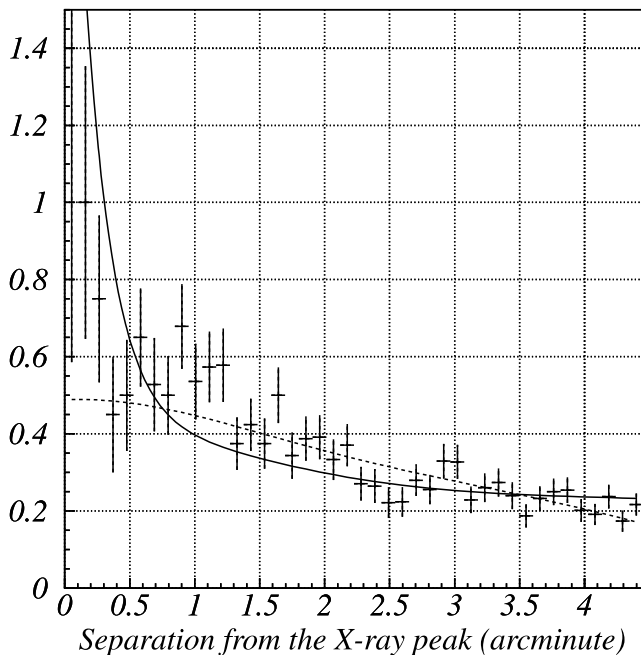

FIG. 3.—SIS radial profile of X-ray intensity in the energy range of (*a*) 6.2–6.6 keV and (*b*) 4.0–10.0 keV (excluding the 6.2–6.6 keV band). The radial profile of the PSF is shown by the solid line, while the simulated XRN profile (see § 4.3) after the convolution of PSF is given by dotted lines.

best-fit reduced χ^2 to be 1.75 (40 dof) for the 6.4 keV line and 3.46 (40 dof) for the continuum band. These reduced χ^2 values exclude the possibility of Sgr B2 being a point source. The observed radial profile and the PSF are shown in Figure 3.

It is conceivable, though, that significant fractions of X-rays from a point source near or behind the GC region are scattered by dust grains and produce an X-ray halo, which mimics this source to be an extended object. Within the *ASCA* spatial resolution, however, no point sources near the GC region are found to be extended, as is demonstrated in Maeda et al. (1996) and Sakano et al. (1999). Thus, scattering by interstellar dust is negligible.

Since the column density to Sgr B2, $N_H = 8 \times 10^{23}$ H cm^{-2}, is at least 5 times larger than that of interstellar gas to the GC region (Sakano et al. 1997), the X-ray halo due to dust grains in the Sgr B2 cloud would be more enhanced. With a distance D to a point source, a halo size by dust scattering at the Sgr B2 cloud is estimated to be $2.7 \times$ (1–8.5 kpc/D) (Xu, McCray, & Kelly 1986; Mitsuda et al. 1990), while the scattered X-rays in the halo are estimated to be about 25% of the direct beam (Mathis & Lee 1991; Mauche & Gorenstein 1986). Taking an extreme case, where a point source is at the infinite distance to make the scattered halo the most extended, we simulated the *ASCA* profile of a point source plus X-ray scattered halo and fitted it to the observed profile. This hypothesis still leads to smaller extension than observed and is excluded with the best-fit reduced χ^2 of 1.45 (40 dof) and 2.84 (40 dof) for the 6.4 keV and continuum bands, respectively.

We thus conclude that the extended structure we observed is not due to an X-ray halo of a point source, but is an intrinsic feature of the Sgr B2 cloud.

4. X-RAY REFLECTION NEBULA

In § 3 we (1) confirmed the presence of the very strong emission line at 6.4 keV; (2) found a large low-energy cutoff and a deep absorption edge at 7.1 keV, both requiring an extremely large column near or at the Sgr B2 cloud; and (3) found that the X-ray–emitting region is extended with its peak position about 1′–2′ offset from the cloud center to the GC side.

This peculiar X-ray spectrum and morphology are attributable to Thomson scattering (continuum emissions), photoelectric absorption of neutral iron atoms (low-energy cutoff and iron K edge), and fluorescence (6.4 keV line) produced by an irradiation of an external X-ray source. We refer to this scenario as the "X-ray reflection nebula" (XRN) model. This section is devoted to numerical simulations to see whether the XRN model reproduces the X-ray spectrum and morphology of Sgr B2.

4.1. *Numerical Simulations*

The geometry and configuration for XRN simulations are given in Figure 4, with the following assumptions:

1. A model cloud (an XRN) is cylindrically symmetric with its axis parallel to our line of sight. The mass distribution of the cloud is taken from the result of ^{13}CO and the $C^{18}O$ observations by Lis & Goldsmith (1989):

$$\left(\frac{n_{H_2}}{1 \text{ cm}^{-3}}\right) = 5.5 \times 10^4 \left(\frac{r}{1.25 \text{ pc}}\right)^{-2} + 2.2 \times 10^3, \quad (1)$$

where n_{H_2} is the number density of hydrogen molecules, and r is the projected distance from the center of the cloud. This
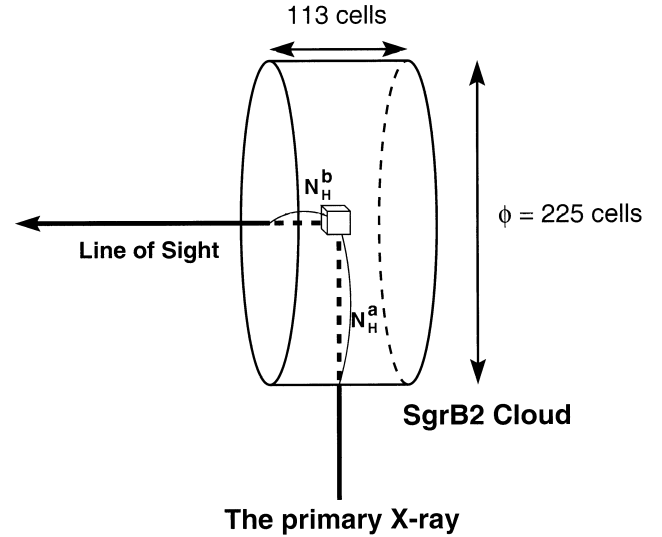

FIG. 4.—Schematic view of the XRN simulation (see § 4)

formula gives the total molecular mass to be $6.3 \times 10^6 M_\odot$ in the 45 pc diameter region.

2. A primary (irradiating) source is located in the GC side with the normal angle to the cloud (cylinder) axis. The spectrum of the primary source is a power law with a photon index of 2 (Koyama et al. 1996).

For numerical simulations, we divided the model cloud into $225 \times 225 \times 113$ cells (each cell is 0.2 pc in size) and calculated absorbed, reflected, and fluorescent X-rays in each cell as a function of incident X-ray energy (E) from the primary source. For simplicity we adopted further assumptions.

3. The reflection and fluorescence are isotropic, and the absorption is given by the analytical function of the photoelectric cross section for the standard interstellar matter (Morrison & McCammon 1983). The cross section of an iron atom was taken from Henke et al. (1982).

4. Since the Thomson scattering optical depth is much smaller than that of the photoelectric absorption in the relevant energy band below 10 keV, we neglect the multiple Thomson scattering.

Then the probability $P_{scat}(E)$ that a primary X-ray photon arrives at a cell, is scattered, and comes into our line of sight is given as a function of photoelectric absorption cross section [$\sigma(E)$], the column density from the primary source to the cell (N_H^a), the cell size (l), Thomson scattering cross section (σ_T), the H number density in the cell (n_{cell}), and the column density from the cell to the surface of the cloud (N_H^b) (see Fig. 4):

$$P_{scat} = l n_{cell} \sigma_T \exp\left[-N_H^a \sigma(E) - N_H^b \sigma(E)\right]. \quad (2)$$

Some fraction of the primary X-rays with energies above 7.1 keV, the K edge of neutral iron, are absorbed with the cross section of an iron atom [$\sigma_{Fe}(E)$]. The absorbed X-rays are reemitted as the 6.4 keV photons, with the probability of the fluorescence yield of 0.34 (Bambynek et al. 1972).

Thus, the probability $P_{6.4}$ that a primary X-ray ($E \geq 7.1$ keV) is converted to the 6.4 keV line and comes into our line of sight is similarly given,

$$P_{6.4} = 0.34 l n_{cell} Z_{Fe} \sigma_{Fe}(E) \exp\left[-N_H^a \sigma(E) - N_H^b \sigma(6.4)\right], \quad (3)$$

where Z_{Fe} is the abundance of iron.

In both the cases, the interstellar absorption from the primary source to the cloud is neglected. Adopting the Galactic absorption from the cloud to the observer of 1×10^{23} H cm^{-2} (Sakano et al. 1997), we finally obtained simulated spectra and images in the continuum and the 6.4 keV line bands.

4.2. Spectrum

The simulated spectra are convolved with the response function and are compared with the observed spectrum. We first fitted the observed spectrum to the simulated one with the XRN model of solar abundances, where a free parameter is only the normalization of the flux.

This simulated spectrum, however, is rejected with a reduced χ^2 of 2.35 (36 dof). Large residuals are found in the flux of the 6.4 keV line, depth of the K edge, and low-energy absorption. We accordingly vary the abundances collectively, fixing the relative ratio to be solar. We find an acceptable fit with the reduced χ^2 of 1.18 (35 dof), when the abundances are 2.2 solar.

Since we have already found the deep edge of iron at 7.1 keV, we further search for a better XRN model, allowing the iron abundance to be an additional free parameter, and find a better fit with the reduced χ^2 of 0.78 (34 dof). The best-fit XRN spectrum is given in Figure 2 by the solid line. The abundances of iron and the others are determined to be 2.4 and 1.6, respectively, while the 90% error contour is given with the solid-line ellipse in Figure 5a (see §§ 4.3, 4.4).

4.3. X-Ray Images

With the same procedure for the XRN spectral model, we simulate XRN images of the 6.4 keV fluorescent line (Fig. 6) and the continuum. The XRN images are convolved with the PSF produced by the ray-tracing code (Kunieda et al. 1995). Then we make radial profiles of the XRN model and fit to the observed profiles given in Figure 3. Allowing normalization and background level as two free parameters, we get acceptable fits with the reduced χ^2 values of 1.25 (40 dof) for the 6.4 keV line and 1.06 (40 dof) for the continuum X-rays. The best-fit curves are shown in Figure 3 with the dotted lines.
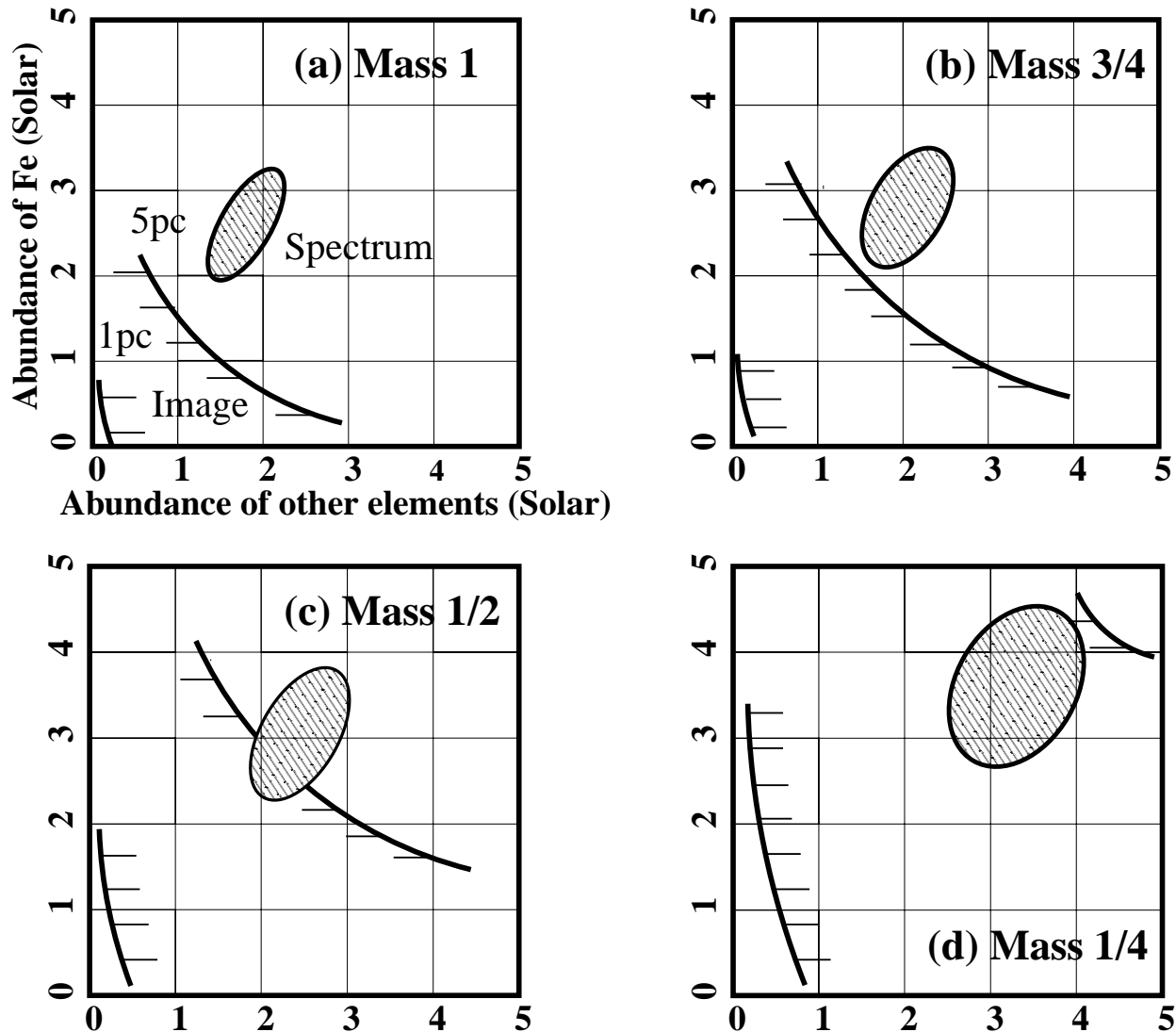

FIG. 5.—The 90% confidence contours for the abundances of iron and other elements obtained by the spectrum analysis under the four assumptions of the total mass: (a) 6.3×10^6, (b) 4.7×10^6, (c) 3.2×10^6, and (d) 1.6×10^6 in unit of solar mass; each corresponds to 1, $\frac{3}{4}$, $\frac{1}{2}$, and $\frac{1}{4}$ of the estimation of Lis & Goldsmith (1989). The constant-separation lines for the 1 pc and 5 pc between the 6.4 keV X-ray peak and the molecular core are also illustrated in each case.
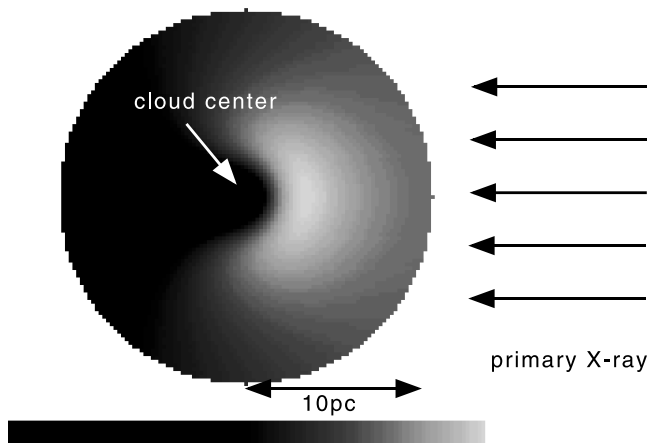
FIG. 6.—Simulated XRN image of the 6.4 keV line. The brightest region is shifted from the cloud center to the side of the primary X-ray source.

Since the radial profile is less sensitive to the abundances and we already obtained acceptable fits with the solar abundances, no significant constraint on the abundances is given. Hence, we try to give possible constraint on the abundances using the separation angle between the 6.4 keV X-ray peak and the cloud core, because larger absorption in the molecular cloud gives further shift of the 6.4 keV peak to the primary source side.

The observed 6.4 keV peak is 3 ± 2 pc away from the radio peak. We thus make constant-separation lines of 1 pc and 5 pc by XRN models, allowing abundances of iron and the other elements to be free parameters. The results are given in Figure 5a (see § 4.4) with solid lines. We find, however, no overlapping region in the abundances of iron and the other elements between those estimated with the XRN spectrum and images (separation angle).

4.4. Mass and Abundance

The disagreement of the best-fit abundances between the XRN images and spectrum may be attributable to an improper assumption on the gas distribution for the Sgr B2 cloud, in either the shape, total gas mass, or probably both. However, for simplicity we make XRN spectra and images and fit the data allowing the total gas mass and abundances to be free parameters.

Consistent results are obtained by reducing the total gas mass to be less than half of the initial gas assumption of Lis & Goldsmith (1989). For example, we show the case of total

TABLE 2
Comparison between Required Luminosities and Those Observed

X-Ray Binary Sources	d^a (pc)	L_{obs}^b (ergs s^{-1})	L_{req}^c (ergs s^{-1})
A 1742−294	170	2×10^{36}	9×10^{39}
1E 1740.7−2942	233	4×10^{36}	2×10^{40}
1E 1743.1−2843	63	1×10^{36}	1×10^{39}

[a] Projected distance to Sgr B2.
[b] Observed luminosity in the 2–10 keV band (Sidoli et al. 1999).
[c] Required luminosity to account for the observed X-ray fluxes of Sgr B2.

gas mass of 1, $\frac{3}{4}$, $\frac{1}{2}$, and $\frac{1}{4}$ of Lis & Goldsmith (1989) in Figure 5. The allowable regions are given by solid lines and ellipse of each graph. We constrain the total mass and the abundance of this cloud to be less than $3 \times 10^6 \, M_\odot$ and greater than 2 solar, respectively.

Thus, the X-ray reflection nebula scenario has the potential to determine the total gas mass and chemical abundances. However, since the observed value of the peak separation still has a large error, further study along this approach should be postponed until high-quality data in morphology and spectroscopy become available.

4.5. Irradiating Source

Using the best-fit parameters given in Figure 5 and from equations (2) and (3), we calculate the fractions of the reflected and fluorescent fluxes and estimate the required luminosity of the primary source to give the observed fluxes of continuum X-rays and the 6.4 keV photons. The required luminosity of the primary X-ray source is

$$L_{2-10 \, keV} \sim 3 \times 10^{39} \left(\frac{d}{100 \, pc} \right)^2 \, ergs \, s^{-1} , \quad (4)$$

where d is the distances from the primary X-ray source to Sgr B2. Since the reflecting region is extended largely over the Sgr B2 cloud, the required X-ray flux should be the value averaged over a time of about 100 yr. This may exclude Galactic binary transient sources as the primary X-ray, whose duty cycle of flaring may be very short. Hence we compare the required flux with the observed luminosities of rather stable sources found in the catalog near the GC in Table 2 (Sidoli et al. 1999).

The observed luminosities of cataloged bright X-ray sources near the GC are $(1–4) \times 10^{36}$ ergs s^{-1}, which are much lower than that required to explain the reflected luminosity of Sgr B2.

5. DISCUSSION

Our interpretation of Sgr B2 as an XRN is supported by the numerical simulation stated in § 4. The model explains well the spectrum and morphology of Sgr B2, and we can constrain the mass and the abundances of this cloud to be less than $3 \times 10^6 \, M_\odot$ and greater than 2 solar, respectively. Since Sgr B2 is located near the GC, the chemical abundances would be similar to those of the GC region. It has been debatable whether the GC region is overabundant or not (Binette et al. 1982; Luck 1982; Shaver et al. 1983; Ratag et al. 1992; Sellgren, Carr, & Balachandran 1997; Ramirez et al. 1999). Our result favors the overabundance for the GC region.

The total gas mass of the Sgr B2 has been poorly known. Oka et al. (1998) presented two possibilities about the mass in the 42 pc diameter region to be either $7.1 \times 10^6 \, M_\odot$ or $2.0 \times 10^5 \, M_\odot$, depending whether the cloud is in self-gravitational equilibrium or is in pressure equilibrium with the hot gas and/or the magnetic field near the cloud region. The former estimation is supported by Lis & Calstrom (1994) for instance, who claimed the mass to be $2 \times 10^6 \, M_\odot$ based on the observation of 800 μm dust emission. Our result, on the other hand, favors the latter estimation. This apparent inconsistency is conceivable if the central dense core of the Sgr B2 is in the self-gravitational equilibrium and the outer part is in the pressure equilibrium.

We find no X-ray source that exhibits enough X-rays to produce the flux of possible XRN, Sgr B2. Koyama et al. (1996) pointed out that the hot plasma prevailing in the GC region can explain only 10% of the Sgr B2 flux. Thus, one plausible possibility, as already proposed by Koyama et al. (1996), is that the Galactic nucleus Sgr A* was bright some hundreds of years ago, the light-travel time between Sgr A* and Sgr B2, and is dim at present.

Sunyaev & Churazov (1998) simulated the morphology of the surface brightness distribution, the equivalent width, and the shape of the fluorescent line from the Sgr B2 cloud as a function of time and relative position of the XRN, and the primary (irradiating) source. They examined both the cases of a flarelike and a step-function (X-ray flux is constant, but suddenly decreases to zero) irradiation by an X-ray source. As they demonstrated, a short time variability is the key to investigate the nature of the irradiating source, whether it is the Galactic nucleus or a binary X-ray source. For comparison with data, observations with higher angular resolution are necessary. The *Chandra* resolution of $0''.5$, for example, can attain the time resolution of about 1 month, which is a typical flare duration of a transient binary. Future observations may thus reveal more realistic two-dimensional gas distribution.

If Sgr A* was a bright X-ray source in the past, we can expect molecular clouds other than Sgr B2 to also be 6.4 keV sources. The X-ray bright spot near the radio arc is such a candidate. Sgr C at the similar distance of Sgr B2 from Sgr A* (on the other side of the center), however, is not distinctly bright in the 6.4 keV line (Koyama et al. 1996). The mass of the Sgr C cloud is about $\frac{1}{7}$ of Sgr B2 (Oka et al. 1998), hence the luminosity is also $\frac{1}{7}$. Thus, whether the Sgr C is an XRN is unclear with the present photon statistics. High-quality X-ray and radio data of the cloud are crucial to judge the XRN scenario, to search for past activities of the GC region and Sgr A*, or to investigate the mass distribution and abundances of the molecular cloud.

6. SUMMARY

The *ASCA* observations highlight peculiar characteristics of the giant molecular cloud Sgr B2, and our analysis supports an interpretation that the cloud is an XRN. The observational facts and their implications are the following:

1. We find a strong emission line at 6.4 keV from cold iron with an equivalent width of about 2.9 keV. No significant emission line from He-like iron, which is commonly observed near the GC region, is found from Sgr B2.

2. The spectrum exhibits a large absorption at energies lower than 4 keV, equivalent to the hydrogen column of 8×10^{23} H cm^{-2} (with the solar abundances) and a pronounced edge structure at 7.1 keV with equivalent iron column N_{Fe} of 4×10^{19} Fe cm^{-2}.

3. The X-ray image of the 6.4 keV line as well as the continuum band is found to be extended with the peak shifted toward the GC by about $1'-2'$.

4. The spectrum and the X-ray morphology are well reproduced by an XRN model, in which a strong X-ray source is irradiating the molecular cloud Sgr B2 from the GC direction.

5. The XRN model favors an overabundance and smaller total gas mass of the Sgr B2 cloud.

6. No X-ray source luminous enough to produce the XRN is found. One possibility is that the past activity of the GC is responsible for the presence of reflected X-rays and absence of the irradiating source at present.

REFERENCES

Bally, J., Stark, A. A., Wilson, R. W., & Henkel, C. 1988, ApJ, 324, 223
Bambynek, W., Crasemann, B., Fink, R. W., Freund, H.-U., Mark, H., Swift, C. D., Price, R. E., & Rao, P. V. 1972, Rev. Mod. Phys. 44, 716
Binette, L., Dopita, M. A., D'Odorico, S., & Benvenuti, P. 1982, A&A, 115, 315
Burke, B. E., Mountain, R. W., Harrison, D. C., Bautz, M. W., Doty, J. P., Ricker, G. R., & Daniels, P. J. 1991, Proc. IEEE, 38, 1069
Gotthelf, E. 1996, The *ASCA* News (Greenbelt: NASA/GSFC), 4, 31
Henke, B. L., Lee, P., Tanaka, T. J., Shimabukuro, R. L., & Fujikawa, B. K. 1982, Atomic Data Nucl. Data Tables, 27, 1
Koyama, K., Awaki, H., Kunieda, H., Takano, S., Tawara, Y., Yamauchi, S., & Nagase, F. 1989, Nature, 339, 603
Koyama, K., Maeda, Y., Sonobe, T., Takeshima, T., Tanaka, Y., & Yamauchi, S. 1996, PASJ, 48, 249
Kunieda, H., Furuzawa, A., Watanabe, M., & the XRT Team 1995, The *ASCA* News (Greenbelt: NASA/GSFC), 3, 3
Lis, D. C., & Carlstrom, J. E. 1994, ApJ, 424, 189
Lis, D. C., & Goldsmith, P. F. 1989, ApJ, 337, 704
Lis, D. C., Goldsmith, P. F., Carlstrom, J. E., & Scoville, N. Z. 1993, ApJ, 402, 238
Luck, R. E. 1982, ApJ, 256, 177
Maeda, Y., Koyama, K., Sakano, M., Takeshima, T., & Yamauchi, S. 1996, PASJ, 48, 417
Makishima, K., et al. 1996, PASJ, 48, 171
Mathis, J. S., & Lee, C.-W. 1991, ApJ, 376, 490
Mauche, C. W., & Gorenstein, P. 1986, ApJ, 302, 371
Mitsuda, K., Takeshima, T., Kii, T., & Kawai, N. 1990, ApJ, 353, 480
Morrison, R., & McCammon, D. 1983, ApJ, 270, 119
Ohashi, T., et al. 1996, PASJ, 48, 157

Oka, T., Hasegawa, T., Hayashi, M., Hanada, T., & Sakamoto, S. 1998, ApJ, 493, 730
Ramirez, S. V., Sellgren, K., Carr, J., Balachandran, S., Blum, R. D., & Terndrup, D. 1999, in ASP Conf. Ser. 186, The Central Parsecs of the Galaxy, ed. H. Falcke, A. Cotera, W. Duschl, F. Melia, & M. Rieke (San Francisco: ASP), 373
Ratag, M. A., Pottasch, S. R., Dennefeld, M., & Menzies, J. W. 1992, A&A, 255, 255
Reid, M. J., Schneps, M. H., Moran, J. M., Gwinn, C. R., Genzel, R., Downes, D., & Rönnäng, B. 1988, ApJ, 330, 809
Sakano, M., Imanishi, K., Tsujimoto, M., Koyama, K., & Maeda, Y. 1999, ApJ, 520, 316
Sakano, M., Nishiuchi, M., Maeda, Y., Koyama, K., & Yokogawa, J. 1997, in IAU Symp. 184, The Central Regions of the Galaxy and Galaxies, ed. Y. Sofue (London: Kluwer), 443
Sellgren, K., Carr, J. S., & Balachandran, S. C. 1997, in IAU Symp. 184, The Central Regions of the Galaxy and Galaxies, ed. Y. Sofue (London: Kluwer), 21
Serlemitsos, P. J., et al. 1995, PASJ, 47, 105
Shaver, P. A., McGee, R. X., Newton, L. M., Danks, A. C., & Pottasch, S. R. 1983, MNRAS, 204, 53
Sidoli, L., Mereghetti, S., Israel, G. L., Chiappetti, L., Treves, A., & Orlandini, M. 1999, ApJ, 525, 215
Sunyaev, R., & Churazov, E. 1998, MNRAS, 297, 1279
Tanaka, Y., Inoue, H., & Holt S. S. 1994, PASJ, 46, L37
Xu, Y., McCray, R., & Kelley, R. 1986, Nature, 319, 652
Yamauchi, S., Kawada, M., Koyama, K., Kunieda, H., Tawara, Y., & Hatsukade, I. 1990, ApJ, 365, 532